

# A Textural Record of Solidification and Cooling in the Skaergaard Intrusion, East Greenland

MARIAN B. HOLNESS<sup>1\*</sup>, CHRISTIAN TEGNER<sup>2</sup>,  
TROELS F. D. NIELSEN<sup>3</sup>, GEMMA STRIPP<sup>1</sup> AND  
STEARNS A. MORSE<sup>4</sup>

<sup>1</sup>DEPARTMENT OF EARTH SCIENCES, UNIVERSITY OF CAMBRIDGE, DOWNING STREET, CAMBRIDGE CB2 3EQ, UK

<sup>2</sup>DEPARTMENT OF EARTH SCIENCES, UNIVERSITY OF AARHUS, HØEGH-GULDBERGS GADE 2, DK-8000 AARHUS C, DENMARK

<sup>3</sup>GEOLOGICAL SURVEY OF DENMARK AND GREENLAND, ØSTER VOLDGADE 10, DK-1350 COPENHAGEN K, DENMARK

<sup>4</sup>DEPARTMENT OF GEOSCIENCES, UNIVERSITY OF MASSACHUSETTS, 611 NORTH PLEASANT STREET, AMHERST, MA 01003-9297, USA

RECEIVED MAY 29, 2007; ACCEPTED OCTOBER 1, 2007  
ADVANCE ACCESS PUBLICATION OCTOBER 25, 2007

*The clinopyroxene–plagioclase–plagioclase dihedral angle,  $\Theta_{cpx}$ , in gabbroic cumulates records the time-integrated thermal history in the sub-solidus and provides a measure of textural maturity. Variations in  $\Theta_{cpx}$  through the Layered Series of the Skaergaard intrusion, East Greenland, demonstrate that the onset of crystallization of clinopyroxene (within LZa), Fe–Ti oxides (at the base of LZc) and apatite (at the base of UZb) as liquidus phases in the bulk magma is recorded by a stepwise increase in textural maturity, related to an increase in the contribution of latent heat to the total heat loss to the surroundings and a reduction in the specific cooling rate at the crystallization front of the intrusion. The onset of both liquidus Fe–Ti oxide and apatite crystallization is marked by a transient increase in textural maturity, probably linked to overstepping before nucleation. Textural maturation at pyroxene–plagioclase–plagioclase triple junctions effectively ceases in the uppermost parts of the Layered Series as a result of the entire pluton cooling below the closure temperature for dihedral angle change, which is  $\leq 1075^\circ\text{C}$ . Solidification of the Layered Series of the Skaergaard intrusion occurred via the upwards propagation of a mush zone only a few metres thick.*

KEY WORDS: magma; partial melting; asthenosphere; olivine; mantle

## INTRODUCTION

Physical and chemical separation of crystals and residual liquid in solidifying magma are the prime controls on the composition, and therefore physical properties, of erupted lavas. It is therefore essential to understand the problems involved in the progressive solidification of large magma bodies in the crust. Solidification of chemically complex silicate magmas involves the development of a crystal mush on the margins of the magma chamber, and it is the formation of these boundary layers that governs the chemical evolution of the remaining magma. Although several recent papers have challenged the concept that solidification at chamber margins can affect the residual liquids (e.g. Marsh, 2006), comprehensive documentation of progressively more fractionated rocks towards the central regions of large intrusions demonstrates the effective separation of early formed crystals from their parental liquids (e.g. Wager & Deer, 1939; Wager *et al.*, 1960). Of crucial importance in this process is the precise timing of the onset of crystallization of each mineral phase within the bulk magma, upon which the liquid line of descent in the evolving magma depends.

\*Corresponding author. Telephone: 01223 333434. Fax: 01223 333450. E-mail: marian@esc.cam.ac.uk

Our understanding of cumulate rocks is based on the concepts first propounded by Wager *et al.* (1960), who suggested that the mushy zone on the magma chamber floor is built of gravitationally separated crystals nucleated and grown in the bulk liquid. These cumulus crystals subsequently undergo further post-accumulation growth, accompanied by the nucleation and growth of other phases, from the intercumulus liquid in the mush. Following challenges to the concept of crystal settling (or flotation) in favour of *in situ* growth on the chamber floor (e.g. Campbell, 1978), Irvine (1982) refined this concept, retaining the term cumulus to describe early crystallizing euhedral to subhedral crystals that form a framework.

The classical textural criteria first proposed by Wager *et al.* (1960) for determining which mineral phases were on the liquidus (i.e. have cumulus status) are not always reliable (e.g. Hunter, 1987). In the case of the Skaergaard intrusion of East Greenland, clinopyroxene growth is dominated by poikilitic habit in the lower parts of the stratigraphy even while it is nucleating in the bulk of the liquid, potentially leading to misinterpretation of crystallization history (McBirney & Noyes, 1979; McBirney & Hunter, 1995; Morse, 1998; Holness *et al.*, 2007a). The importance of accurate identification of the bulk liquidus assemblage becomes acute when considering whether basaltic liquids follow a trend of progressive Fe enrichment (the Fenner trend) or Si enrichment (the Bowen trend). An example of this is provided by the ambiguity that surrounds the textural status of Fe–Ti oxides in the Skaergaard intrusion and the consequent difficulties for interpretation of the liquid line of descent (Wager, 1960; Hunter & Sparks, 1987, 1990; Brooks & Nielsen, 1990; McBirney & Naslund, 1990; Morse, 1990; Hanghøj *et al.*, 1995; Tegner, 1997; Irvine *et al.*, 1998).

Regardless of whether the mush accumulated by gravitational separation of cumulus grains, or by *in situ* growth of primocrysts, the distinction between early formed and later phases, first identified by Wager *et al.* (1960), is very clear in coarse-grained, mafic, glassy crystalline nodules entrained in lava flows (Fig. 1a and b). These show that the mush develops by the infilling of original liquid-filled pores in a primocryst framework by later crystallizing phases (Holness *et al.*, 2005, 2007b). The pseudomorphing of the pore spaces by these interstitial phases provides us with a new interpretative tool.

Preliminary work has shown that systematic changes in the relative loss of latent heat from the mush are recorded in the details of grain boundary orientation at the junctions between primocryst and interstitial grains in a fully solidified cumulate (Holness *et al.*, 2007a). The extent to which interstitial phase–primocryst–primocryst triple junctions have moved away from the initial geometry

inherited from the pseudomorphed liquid phase towards solid-state textural equilibrium (Fig. 1) provides a quantitative measure of the textural maturity. Variations in textural maturity of gabbroic cumulates record the arrival of fresh magma in the chamber, the onset of chamber-wide convection and changes in the liquidus assemblage (Holness *et al.*, 2007a). Grain boundary orientations at triple junctions thus provide hitherto inaccessible information on the development of the crystal mush and hence the chemical evolution of the magma remaining in the chamber.

In this contribution, we build on the work of Holness *et al.* (2005, 2007a) and present the variation of textural maturity through the entire Layered Series of the Skaergaard intrusion. We demonstrate that the sequential arrival of phases on the liquidus is recorded by variations in grain boundary orientation at clinopyroxene–plagioclase–plagioclase junctions, permitting the onset of cumulus crystallization of each phase to be placed in the stratigraphy with great accuracy. We also show that textural maturation (as recorded by clinopyroxene–plagioclase–plagioclase dihedral angles) effectively ceases during the latest stages of crystallization of the intrusion. The estimate this provides of the closure temperature for dihedral angle change constrains the thickness of the crystal mush on the chamber floor to be of the order of a few metres.

## TEXTURAL MATURATION

Textural equilibrium represents the state in which the internal energy incorporated in crystals and their interfaces is minimized. Because textural equilibration is a diffusive process, the extent to which poly-mineralic rocks approach textural equilibrium is a function of their thermal history. At textural equilibrium, all grain boundaries and interfaces have constant mean curvature (Thomson, 1887; Bulau *et al.*, 1979). Furthermore, the relative orientations of grain boundaries and interfaces at three-grain contacts are defined by the relative magnitudes of the interfacial energies via the equation

$$\sum_{i=1}^3 \left( \gamma_i \mathbf{t}_i + \frac{\partial \gamma_i}{\partial \mathbf{t}_i} \right) = 0 \quad (1)$$

where  $\gamma_1$ ,  $\gamma_2$ ,  $\gamma_3$  are the interfacial energies,  $\mathbf{t}_i$  is the vector in the plane of the *i*th surface, normal to the line of intersection of the surfaces and pointing away from this line, and  $\gamma_i / \mathbf{t}_i$  is a vector perpendicular to  $\mathbf{t}_i$  and to the line of intersection (Herring, 1951). For the specific case of a three-grain, two-phase, contact (such as that between two grains of plagioclase and one of pyroxene), or a two-phase contact between two grains of solid and a liquid, the angle defined by equation (1) is known as the dihedral angle.

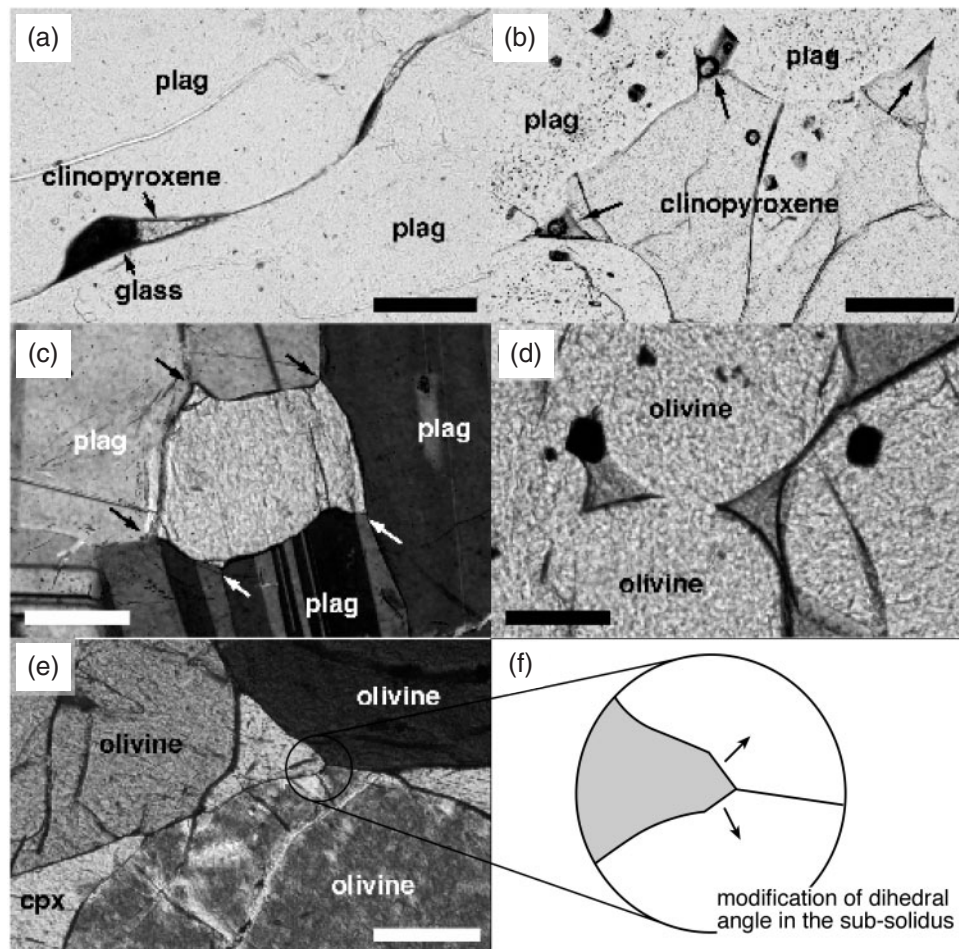


**Fig. 1.** (a) Two glass-filled pores on a plagioclase–plagioclase grain boundary partially filled by clinopyroxene. The smoothly curved boundaries, demonstrating that the clinopyroxene pseudomorphs the pore space, should be noted. Glassy nodule entrained in basalt, Iceland. Scale bar represents 100  $\mu\text{m}$ . Plane-polarized light. (b) Clinopyroxene grain surrounded by plagioclase in a glassy nodule from Mauna Loa, Hawaii. The triangular glass-filled pores (arrowed) formed by the impingement of the plagioclase grains should be noted. The pyroxene grain is growing into these pores. Scale bar represents 200  $\mu\text{m}$ . Plane-polarized light. (c) Cumulus clinopyroxene surrounded by cumulus plagioclase. The triangular extensions of pyroxene at each plagioclase–plagioclase junction (arrowed), formed by the pseudomorphing of the triangular pores shown in (b), should be noted. Gabbro, Rum Eastern Layered Intrusion. Scale bar represents 200  $\mu\text{m}$ . Partially crossed polars. (d) Olivine primocrysts in a glass nodule from Mauna Loa, Hawaii. The rounded shape and establishment of the equilibrium liquid–olivine–olivine dihedral angle should be noted. Scale bar represents 200  $\mu\text{m}$ . Plane-polarized light. (e) In this olivine cumulate from the Rum Eastern Layered Intrusion, the original liquid-filled pores have been pseudomorphed by clinopyroxene. The opening of the three-grain junctions as the dihedral angle moves from the inherited low angle [shown in (d)] towards solid-state equilibrium should be noted. This occurs by movement of large areas of grain boundary in the manner of an opening book (f). Scale bar represents 100  $\mu\text{m}$ . Crossed polars.

The tangential component of equation (1) acts to minimize the interfacial area, whereas the normal component acts to rotate the interface towards an orientation with a lower interfacial energy. Hence, in general, the dihedral angle varies with crystalline orientation (Herring, 1951; Laporte & Provost, 2000).

Crystal growth in the presence of abundant liquid commonly results in planar-sided grains, and the early pore geometry in the highly porous mush at the chamber floor is controlled by random crystal juxtaposition to form an impingement texture (Elliott *et al.*, 1997; Holness *et al.*, 2005). If there is no further solidification, the initial

impingement texture will evolve, driven by the minimization of internal energies, towards the melt-present equilibrium texture in which the fluid-filled pores develop constant mean curvature and the equilibrium value of the liquid–solid–solid dihedral angle (Fig. 1d). The growth of interstitial phases, which commonly pseudomorph the liquid-filled porosity (e.g. Platten, 1981; Harte *et al.*, 1991; Holness & Clemens, 1999; Sawyer, 1999, 2001; Rosenberg & Riller, 2000; Holness *et al.*, 2007b), ends the liquid–solid equilibration process. The pseudomorphing interstitial grains inherit the angle subtended at the pore corners, which is somewhere on the continuum between

an impingement texture (median value  $\sim 60^\circ$ , Elliott *et al.*, 1997; Holness *et al.*, 2005) and a completely equilibrated liquid–solid–solid angle (median value  $< 40^\circ$ , Holness, 2006, and references therein). These angles are much lower than the median solid–solid angles for poly-mineralic silicate rocks, which are  $100\text{--}130^\circ$  (Kretz, 1966; Vernon, 1968, 1970; Holness *et al.*, 2005). The sub-solidus evolution of an orthocumulate texture must therefore involve a general increase in the angle subtended at the corners of pseudomorphed pores (Fig. 1e and f) together with grain boundary migration to achieve constant mean curvature of all boundaries and interfaces [N.B. the term sub-solidus, as used here, refers to the local absence of liquid at the three-grain junction of interest, rather than the complete absence of melt from the rock. This means that for phases that grow over a temperature interval, an additional (temporal) source of angle variability will be superimposed on the variability inherited from the impingement texture (Holness *et al.*, 2005)]. Further textural maturation requires grain growth (e.g. Boorman *et al.*, 2004; Higgins, 1998) which minimizes the total interfacial area. The extent to which a rock, either liquid-bearing or fully solidified, has evolved from the initial texture formed by reaction (or, in the case of cumulates, solidification) towards textural equilibrium provides an indication of the time-integrated thermal history in the sub-solidus.

Holness *et al.* (2005) demonstrated that the first visible change during textural maturation is the alteration of inherited dihedral angles by the rotation of large areas of grain boundary in the manner of an opening or closing book (Fig. 1e and f; Holness *et al.*, 2005). This results in a step-change of the grain boundary curvature some distance from the triple junction (Fig. 1e and f) and it is the outwards propagation of this break in slope that results in the establishment of the new, solid-state equilibrium constant mean curvature. Quantification of progressive changes in grain boundary curvature presents a challenging problem, but the earliest stages of textural maturation can be easily quantified using the dihedral angle. Typically this involves an increase of the median (and mean) of the dihedral angle population from  $\sim 60^\circ$  (with a standard deviation of  $\sim 25^\circ$ ) towards one of  $\sim 120^\circ$  (and a standard deviation of  $\sim 15^\circ$ ) (Holness *et al.*, 2005). Importantly, the process of textural maturation in kilometre-scale mafic intrusions in the shallow crust has an effective closure temperature close to the solidus (Holness *et al.*, 2005), precluding even the attainment of equilibrium solid-state dihedral angles let alone changes in grain shape as a result of the establishment of the new constant mean curvature. The extent to which the dihedral angles have changed in these relatively rapidly cooled intrusions thus provides information about processes occurring at or near the magma–mush interface.

## GEOLOGICAL SETTING

The Skaergaard intrusion forms part of a group of gabbroic and syenitic bodies found in East Greenland and formed during the opening of the Atlantic at about 55 Ma (Deer, 1976; Brooks & Nielsen, 1982; Tegner *et al.*, 1998). It formed by the intrusion of a large ( $8\text{ km} \times 11\text{ km} \times 4\text{ km}$ , Nielsen, 2004) body of relatively evolved tholeiitic basaltic magma at the contact between underlying Precambrian gneisses and an overlying sequence of Tertiary plateau lavas (Fig. 2). The thickness of the overlying lavas increased during the solidification of the intrusion, which evolved from a subvolcanic magma chamber ( $0.7 \pm 0.5\text{ kbar}$ ) to a more deep-seated system ( $3.3 \pm 1.3\text{ kbar}$ ) as it crystallized (Larsen & Tegner, 2006). Once the chamber was filled, it fractionated as a closed system to form the prime example of shallow magmatic differentiation.

Tilting of the eastern coast of Greenland by about  $20^\circ$  (Wager & Brown, 1968; McBirney, 1996), associated with regional stretching, has resulted in the almost continuous exposure of  $> 3.5\text{ km}$  of stratigraphy, which dips gently to the SE. Wager & Deer (1939) divided the exposed part of the intrusion into three major units: the Layered Series, formed on the floor of the intrusion; the Marginal Border Series, crystallized inwards from the walls; and the Upper Border Series, which grew downwards from the roof. The Hidden Zone (HZ) is that part of the Layered Series underlying the lowermost exposed horizons. The Layered Series meets the Upper Border Series at the so-called Sandwich Horizon (Wager & Deer, 1939), which represents the last parts of the intrusion to solidify. The Layered Series, with which this contribution is concerned, is subdivided into Lower, Middle and Upper Zones by the disappearance of abundant olivine primocrysts at the base of Middle Zone and their reappearance at the base of the Upper Zone. The Lower Zone is further divided into three subzones: LZa, in which cumulus phases are olivine and plagioclase, with clinopyroxene joining the assemblage near the top; LZb, the base of which is marked by a change in clinopyroxene habit from poikilitic to granular; and LZc, which is marked by the appearance of cumulus Fe–Ti oxide minerals. The Upper Zone is also subdivided into three: the base of UZb is marked by the appearance of abundant apatite primocrysts, and the base of UZc is defined by the appearance of a mosaic formed of ferrohedenbergite inverted from  $\beta$ -ferrobustamite. Layering, defined by variations in modal composition and by a weak preferred alignment of tabular plagioclase grains, is present throughout the Layered Series up to the middle of UZb (Wager & Brown, 1968; Irvine *et al.*, 1998).

The division between LZa and LZb, defined as the (clearly visible in outcrop) change from poikilitic to granular habit of the clinopyroxene, occurs at 175 m stratigraphic height (measured assuming a zero point at the base of the exposed Layered Series, after Wager & Deer, 1939).

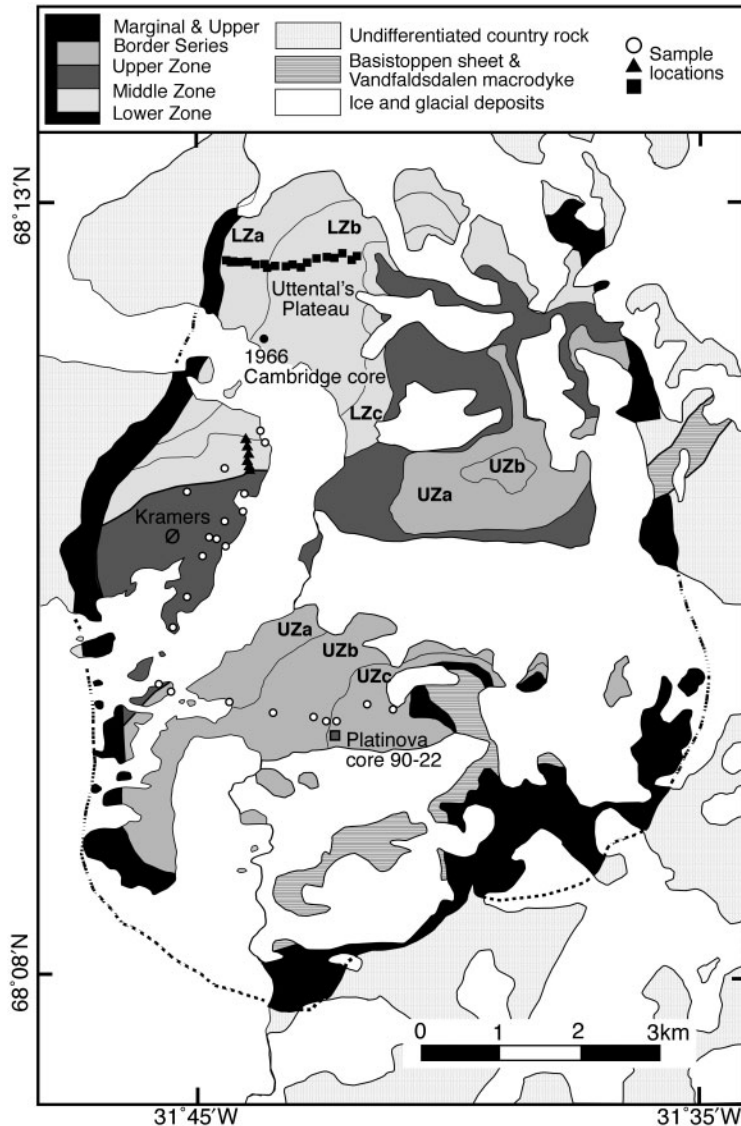


**Fig. 2.** Simplified geological map of the Skaergaard intrusion (after McBirney, 1989) showing the location of the two drill cores and the sample sets. Symbols as in Fig. 4.

Although this change in habit was assumed by Wager & Brown (1968) to indicate the onset of clinopyroxene crystallization as a liquidus phase, Holness *et al.* (2007a) showed that clinopyroxene joined the liquidus assemblage at 100 m stratigraphic height above the lowest exposed horizons, as recorded by a step-change in the textural maturity. This is in agreement with Nwe (1976), who placed on the arrival of cumulus clinopyroxene at 110 m in the Cambridge 1966 drill core on the basis of pyroxene grain shape.

### LOCATION OF SAMPLES

The samples comprise several different sets, as follows. (1) A suite collected by Karen Bollingberg (Bollingberg, 1995)

and housed at GEUS, Copenhagen. This comprises samples from LZa up to the Sandwich Horizon, collected along a traverse of Kramers Ø and on the mainland west of Basistoppen. (2) A suite collected in 2000 by Christian Tegner and others, comprising several traverses across the intrusion covering the entire exposed stratigraphy of the Layered Series (Nielsen *et al.*, 2000; housed at Aarhus University). (3) The Cambridge drill core, collected in 1966 by W. A. Deer and G. A. Chinner from the unexposed base of the intrusion (Maaløe, 1976; Holness *et al.*, 2007a), through the Hidden Zone up to LZb. It is housed at the University of Cambridge. (4) A 950 m long drill core, numbered 90-22, collected by Platinova Resources Ltd. in 1990, which covers the upper part of MZ up to UZc

Table 1: Average thickness of units and their proportion of the total mass of the intrusion from Nielsen (2004)

Zone	Average thickness (m)	Mass proportion
HZ	325	11.29
LZa	375	12.84
LZb	650	16.65
LZc	250	5.44
MZ	480	9.79
UZa	400	7.24
UZb	400	5.94
UZc	150	1.38
Upper Border Series	600	13.29
Marginal Border Series	350	16.31

The original model considered HZ and LZa as a single unit (totalling 700 m), but here we divide the 700 m according to the proportions observed in the Cambridge 1966 drill core.

(Tegner, 1997; housed at GEUS in Copenhagen). Sample locations are shown in Fig. 2.

Correlation between the sample sets, to create a single stratigraphic sequence, is not straightforward as the thickness of the subdivisions of the Layered Series varies with position in the intrusion (McBirney, 1996). Thus although the spacing between samples collected from outcrop can be calculated from locally observed layering orientations, the relevance of a unified stratigraphy pieced together from a traverse with a significant along-strike component (such as the Bollingberg suite) is open to question.

We use a reference stratigraphic section through the Skaergaard intrusion calculated from a field-based structural reconstruction (Nielsen, 2004). This results in the average thicknesses of the subzones shown in Table 1 [taken from the lower left-hand column of Appendix 4 of Nielsen (2004)]. The sample sets were placed within the stratigraphy using a linear stretching or compression within each zone so that zone boundaries correspond to those of the standardized section. The Nielsen reconstruction groups the Hidden Zone and LZa into a single unit of total thickness 700 m. The Cambridge 1966 drill core contains 150 m of HZ and 175 m of LZa. Using these proportions we divide the 700 m into 325 m of HZ and 375 m of LZa.

## ANALYTICAL METHODS

For incompletely equilibrated samples, and for equilibrated samples in which there is anisotropy of interfacial energies, it is important to obtain direct measurements of the population of dihedral angles using a Universal Stage mounted

on an optical microscope (Kretz, 1966; Vernon, 1968, 1970, 1997; Holness, 2005, 2007; Holness *et al.*, 2005, 2007a). In this manner it is possible to rotate the thin section so that each three-grain junction in turn is oriented so the grain boundaries are parallel to the line of sight, permitting direct measurement of the true angle between the boundaries.

We used a four-axis Leitz Universal Stage, mounted on a James Swift microscope, with a magnification of  $\times 320$ . We measured up to 100 angles in each sample (30 for the most part, reduced to 20 for many samples in MZ, which commonly have late-stage modifications of grain junctions, Stripp *et al.*, 2006). Each measurement gives the angle at the junction between clinopyroxene and two plagioclase grains (the clinopyroxene–plagioclase–plagioclase dihedral angle, or  $\Theta_{\text{cpp}}$ ). The error on each measurement is of the order of a few degrees. Following Holness (2005, 2007) and Holness *et al.* (2005, 2007a) we report the medians of the population for each sample (Table 2; the full dataset is given as the Electronic Appendix, available for downloading from <http://www.petrology.oxfordjournals.org>). The error on the median of the population of measurements from each sample is hard to constrain, but because the median remains within a few degrees for an increasing population once the number of measurements exceeds about 20, we consider that the error on the median value is of the order of  $\pm 2^\circ$ .

## PETROGRAPHY

Although textures record a wealth of information on the structure of the solidifying crystal mush and its physical properties, in this contribution we concentrate on information extracted from the junctions of plagioclase and pyroxene grains (Fig. 3a and b). Both minerals are present throughout the Skaergaard intrusion.

The Skaergaard gabbros contain tabular plagioclase grains that initially formed an initial impingement texture and a framework for the structure of the gabbro. There is no sign of textural equilibration of liquid–plagioclase interfaces. Orthocumulates, formed of primocrystic plagioclase  $\pm$  olivine and interstitial pyroxene, are common in the lower parts of the Layered Series. The rocks develop a more acumulate nature higher in the stratigraphy (Wager *et al.*, 1960).

## Pyroxene

In the lowermost parts of the Layered Series both augite and primary orthopyroxene are present. The orthopyroxene–pigeonite transition is crossed near the base of HZ, leaving coexisting augite and inverted pigeonite for much of LZ (Nwe, 1976). In HZ and LZ, the augites have fine (001), and coarser (100), exsolution lamellae of Ca-poor pyroxene, whereas the inverted pigeonites contain relict '(001)', and fine (100), exsolution lamellae of

Table 2: Median clinopyroxene–plagioclase–plagioclase dihedral angles as a function of (standardized) stratigraphic height

90-22 Platinova drill core			Bollingberg sample set			Tegner 2000 samples		
Depth in core (m)	Height (m)	Median angle	Sample	Height (m)	Median angle	Sample	Height (m)	Median angle
10.6	2905	74.5	SK84-358	1377	105.5	458242	381	78.5
47.4	2879	71.5	SK84-392a	1505	99.5	458212	439	83.5
0.7	2912	76	SK84-356	1278	95.5	458211	338	92.5
67.6	2860	75	SK84-392b	1505	101	458213	505	83
87.7	2841	80	SK84-400	1589	100.5	458245	529	99
107.7	2823	76	SK84-361	1649	101	458214	552	100
170.4	2764	77.5	SK84-403	1693	100	458215	569	100.5
210.9	2727	77	394901	1722	101	458216	591	104
249.2	2691	79.5	SK84-404	1739	101	458217	616	100
270.3	2672	77	394907	1749	101	458218	664	101.5
310.2	2685	80.5	394903	1835	100	458219	668	101.5
328.8	2622	79.5	SK84-406	1858	100.5	458220	694	100
364.1	2585	76	SK84-363	1865	101	458221	698	102
421	2532	75	394904	1872	101.5	458224	703	101.5
429.3	2524	82	394905	1883	101.5	458225	754	101
441.7	2513	90	SK84-409	1936	99.5	458226	837	98
450	2505	89.5	394913	1942	97.5	458227	898	101.5
455	2500	91	SK84-366	1964	100.5	458231	922	100
461.8	2494	91.5	SK84-367	2063	100	458232	988	98.5
467	2489	95	SK84-368	2133	99	458233	1014	91.5
471.8	2485	99	SK84-370	2463	82	458201	1062	99
475	2482	105	SK84-372	2668	78.5	458202	1097	97
481	2477	82	SK84-373	2800	75	458203	1143	96.5
485	2473	80	SK84-374	2820	77	458205	1183	97
491.8	2467	92	SK84-375	2912	79.5	458204	1168	97.5
530.9	2434	95	SK84-376	3003	75.5	458206	1231	99
555.5	2412	96	SK84-377	3027	78	458207	1286	95.5
563.3	2404	97				458276	1286	96.5
585.8	2386	97.5				458277	1310	97.5
660.6	2322	99				458208	1311	97
689.1	2297	100.5				458278	1319	95
729.2	2263	100				458209	1334	94
769.1	2228	99.5				458279	1377	104
809.2	2194	100				458280	1434	103
854.5	2154	101				458283	1478	104
873.7	2138	99.5				458284	1492	101
893.6	2121	99				458285	1517	102
914.2	2103	99.5				458287	1598	102.5
						458288	1600	102

(continued)

Table 2: *Continued*

Cambridge 1966 drill core								
Sample	Height (m)	Median angle	Sample	Height (m)	Median angle	Sample	Height (m)	Median angle
118752	0	75.5	118682	256	82.5	118630	534	83.5
118744	18	78	118681	266	84.5	319'	539	91
118745	18	77.5	118677	280	83.5	320'	534	85
118741	35	76.5	118767	287	79.5	318'	541	96.5
118740	41	80	118675	293	81.5	317'	542	99.5
118738	50	72.5	118673	300	84.5	118629	546	99
118737	56	78	681'1''	306	85.5	118628	552	102.5
118736	63	84.5	671'1''	313	85.5	118626	556	102
118735	68	83	661'2''	319	93	282'4''	565	101.5
118734	71	95.5	651'2''	326	91	272'9''	571	101.5
118733	76	90	118667	329	85	262'7''	578	93.5
118732	79	87.5	631'1''	338	91.5	252'4''	584	107
118731	82	93	621'2''	344	92	118624	591	106.5
118730	89	88	611'1''	351	84	233'	597	101
118729	96	82.5	601'1''	357	86	222'4''	604	101.5
118727	104	84.5	118663	361	82.5	118622	610	101
118726	109	82.5	581'1''	370	83.5	118621	619	100.5
118725	116	84	571'4''	376	80.5	118618	625	103
118723	122	85	561'1''	383	78	118617	629	102
118722	129	86.5	118660	396	78	118616	638	100.5
118717	131	84	522'1''	409	77.5	118615	644	102.5
118714	133	81	511'10''	415	78	118614	649	101
930'2''	142	82	501'1''	421	80.5	118611	657	102.5
920'2''	149	85.5	118645	434	81.5	122'2''	670	100.5
909'11''	155	86	118644	441	80.5	118605	674	101
900'1''	162	87	118643	449	82	101'5''	683	99.5
118709	166	88.5	118642	454	81.5	118596	689	105
879'12''	175	88	118641	460	84	118595	691	103.5
870'2''	181	89.5	118639	469	81	81'1''	696	103
860'2''	188	85.5	118638	479	81	71'1''	703	99
849'10''	195	83	118637	481	83.5	61'1''	706	104
118694	200	81	118636	488	83.5	118594	712	104.5
118693	203	82	118634	494	83.5	118592	717	108
118691	215	86	381'2''	501	81.5	118591	724	101
118689	221	83.5	371'7''	507	82	118589b	726	100
118688	227	85	361'5''	514	83			
118686	235	82	351'7''	520	82.5			
118685	241	83.5	118633	526	82.5			
118684	248	81	118631	533	81			

The full dataset is given as an Electronic Appendix. The data for the Cambridge 1966 drill core were previously reported by Holness *et al.* (2007a).

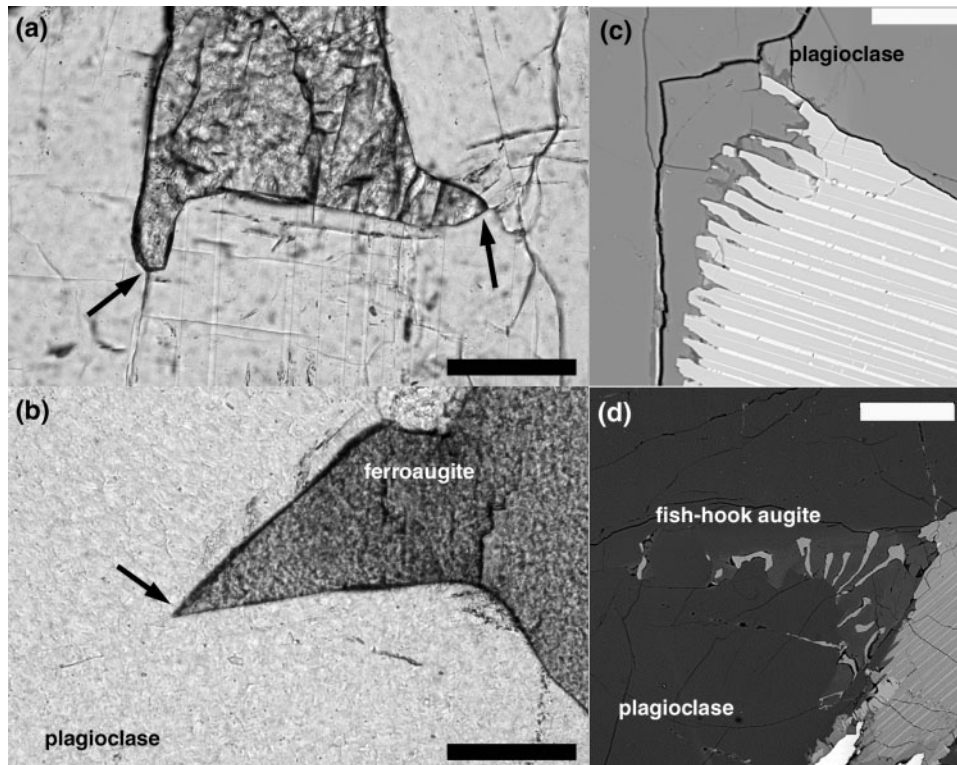


**Fig. 3.** (a) Interstitial augite from LZa, showing changes in grain boundary curvature at clinopyroxene–plagioclase–plagioclase triple junctions (arrowed). Scale bar represents 100  $\mu\text{m}$ . Plane-polarized light. (b) Ferroaugite from UZb showing no deflection of the pyroxene–plagioclase grain boundaries in the vicinity of the three-grain junction (arrowed). Scale bar represents 100  $\mu\text{m}$ . Plane-polarized light. (c) Stepped grain boundaries in MZ. The deep indentations where the Ca-poor exsolution lamellae (pale grey) intersect the pyroxene–plagioclase boundary should be noted. Sample from 1026 m depth in the 90-22 core. Scale bar represents 40  $\mu\text{m}$ . Back-scattered electron image. (d) Fish-hook augites in MZ, forming an intergrowth with An-rich plagioclase (slightly paler grey than the plagioclase primocryst). Sample from 1017 m depth in the 90-22 drill core. Scale bar represents 100  $\mu\text{m}$ . Back-scattered electron image.

Ca-rich pyroxene. Augite is poikilitic in HZ and LZa, although towards the top of LZa grains develop an inclusion-free core signifying the onset of nucleation in the bulk of the magma. Augite has a granular habit through the remainder of the Layered Series. With height, both coexisting pyroxenes become more Fe-rich. By UZa the two cumulus pyroxenes are brown ferroaugite, with fine (20–700 nm) (001) exsolution lamellae (Fig. 3b), and ferropigeonite. The gabbros of UZb contain only a brown ferroaugite, which is joined by a green ferrohedenbergite in UZc.

Above the LZa–b boundary, clinopyroxene–plagioclase grain boundaries have serrations associated with the dissolution of exsolution lamellae of Ca-poor pyroxene, and corresponding growth of the Ca-rich host (Fig. 3c). These serrated, or stepped, boundaries, which are rarely ubiquitous on the thin-section scale, develop gradually with the steps becoming more pronounced, and affecting more boundaries, with stratigraphic height. At their most developed, in MZ, the steps become elongate and irregular (Fig. 3c), commonly associated with vermicular intergrowths of pyroxene and An-rich plagioclase along adjacent plagioclase–plagioclase grain

boundaries (Fig. 3d). Such vermicular intergrowths, or ‘fish-hook augites’, have previously been described by Batiza & Vanko (1985).

In the upper parts of the Layered Series the steps on grain boundaries gradually disappear, becoming progressively shallower and more closely spaced with increasing stratigraphic height. They finally disappear at about 2500 m, in the upper parts of UZb (e.g. Fig. 3b). This disappearance is linked to the reduction in thickness of the exsolution lamellae of Ca-poor pyroxene (Brown, 1957; Bown & Gay, 1960; Copley, 1973; Copley *et al.*, 1974; Champness & Copley, 1976; Copley & Champness, 1975), probably a result of low liquidus temperatures in the highly evolved liquids at this level in the intrusion (Nwe & Copley, 1975).

Exsolution lamellae of Ca-poor pyroxene on (001) planes in augite and ferroaugite are always monoclinic. This is the case even when the host crystal contains (100) orthopyroxene lamellae exsolved below the inversion temperature, and when coexisting crystals of the associated Ca-poor pyroxene have inverted (Bown & Gay, 1960; Champness & Copley, 1976; Copley & Champness, 1975;

Nwe & Copley, 1975). Below the inversion temperature the Ca-poor exsolution lamellae are therefore metastable with respect to an orthorhombic form. The non-ubiquity of the stepped boundaries on a thin-section scale, and their association (at least in MZ) with larger, non-isochemical, symplectic structures, suggests that they form by dissolution of metastable Ca-poor pyroxene and recrystallization of adjacent plagioclase and augite consequent to the introduction of a metasomatizing fluid along grain boundaries (Stripp *et al.*, 2006). This process occurred below the temperature of pigeonite inversion which, for Mg/Fe ratios typical of MZ, occurs at 900–1100°C (Brown, 1972). Two-pyroxene thermometry, using the compositions of the coexisting Ca-poor lamellae within the Ca-rich host crystal with the orthopyroxene–clinopyroxene solvus geothermometer of Brey & Köhler (1990) at  $2.3 \pm 0.8$  kbar (the pressure of MZ crystallization, Larsen & Tegner, 2006) gives a temperature of  $811 \pm 32^\circ\text{C}$ . If exsolution continued after the onset of step formation, this provides a lower temperature bound.

The common association of vermicular outgrowths of augite at clinopyroxene–plagioclase–plagioclase junctions with stepped augite–plagioclase boundaries in MZ means that it is difficult to measure a large population of dihedral angles within a single thin section. However, populations of  $\sim 20$  measurements provide a reasonable estimate of the median. Where present, Ca-poor orthorhombic pyroxenes (which are unaffected by step formation) provide a comparable measure via the orthopyroxene–plagioclase–plagioclase dihedral angle. Measurements of pyroxene–plagioclase–plagioclase dihedral angles in UZ were confined to the brown ferroaugites.

## Plagioclase

Plagioclase is a cumulus, or framework-forming, phase throughout the Layered Series. It forms tabular grains with a variably developed preferred orientation in the plane of the igneous layering (Brothers, 1964). In the lower part of the stratigraphy, plagioclase grains are commonly complexly zoned, with partially resorbed cores. These features disappear at  $\sim 30$  m stratigraphic height (Maaløe, 1976) and have been correlated with the cessation of magma input into the chamber (Holness *et al.*, 2007a).

The average composition of plagioclase cores in the exposed part of the Layered Series changes from  $\text{An}_{68}$  at the base of the Cambridge 1966 drill core [thought to be at, or close to, the floor of the intrusion (Maaløe, 1976)] to  $\text{An}_{25}$  at the Sandwich Horizon (McBirney, 1996).

## DIHEDRAL ANGLE VARIATIONS IN THE LAYERED SERIES

Pyroxene–plagioclase–plagioclase junctions through most of the Layered Series display changes in curvature corresponding to alteration of the apparent dihedral angle from that inherited from the original impingement texture (Fig. 3a). This change in curvature is not apparent in UZc, in which the clinopyroxene–plagioclase grain boundaries show no deflection at the triple junction (Fig. 3b). In these upper reaches of the stratigraphy there has been no alteration of the inherited impingement texture.

The variation in clinopyroxene–plagioclase–plagioclase dihedral angles is shown in Fig. 4. For comparison, the data published earlier from the Cambridge 1966 drill core

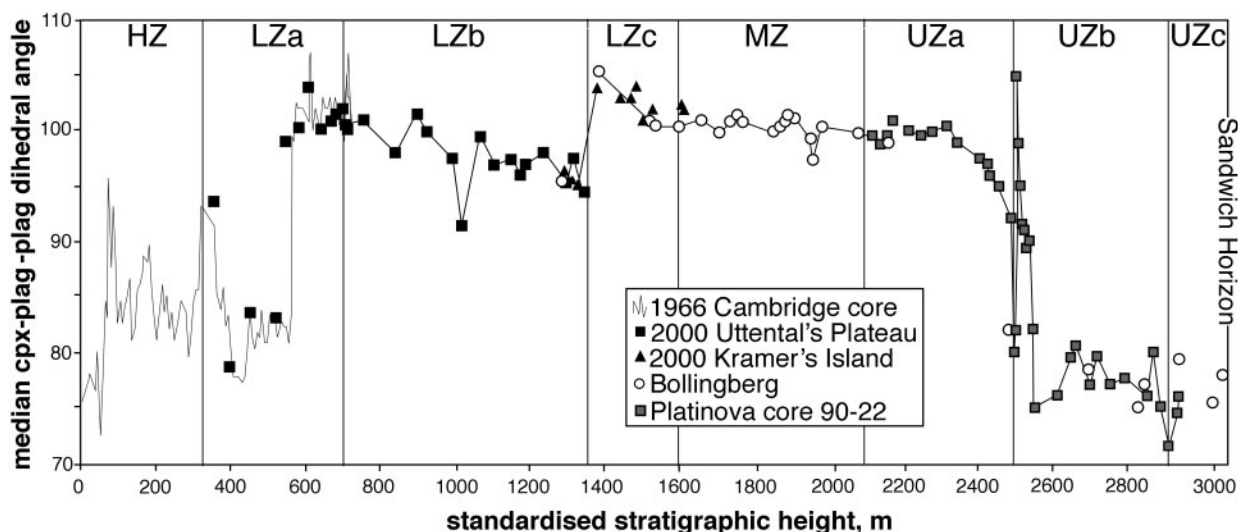


Fig. 4. Median  $\Theta_{\text{cpx}}$  as a function of standardized stratigraphic height through the Layered Series. The location of samples and drill cores is shown in Fig. 2.

and the 2000 Uttentals Plateau suite (i.e. those below the LZa–b boundary) are also included (Holness *et al.*, 2007a). The new data fall between a minimum of 72° and a maximum of 105°, demonstrating an absence of textural equilibrium at clinopyroxene–plagioclase–plagioclase junctions but a substantial variation in the extent to which textural equilibrium has been approached.

In detail, median  $\Theta_{\text{cpp}}$  shows a general decrease in value from about 102° at ~540 m stratigraphic height to about 97° at the top of LZb, a sharp increase to 105° at the base of LZc, followed by a decrease to ~100° through LZc. Within the constraints imposed by the sample density, median  $\Theta_{\text{cpp}}$  appears to be constant through MZ and the lower parts of UZa at ~100°, with much less variability ( $99^\circ < \Theta_{\text{cpp}} < 101^\circ$ , although one sample has a median of 97°). In UZa, median  $\Theta_{\text{cpp}}$  decreases precipitately to 80°, followed by a localized positive excursion at the base of UZb that reaches 105°. The median values of  $\Theta_{\text{cpp}}$  in the remainder of the Layered Series vary in the range 75–80°.

## INTERPRETATION AND DISCUSSION

The data shown in Fig. 4 were collected from a series of traverses from different places across the intrusion. The sample sets overlap at several places in the stratigraphy, with the Bollingberg set covering all the exposed stratigraphy and overlapping with the samples collected by Tegner and others in 2000 and with the 90-22 drill core. It is notable that the dihedral angles at any level in the stratigraphy are constant between the sample sets and demonstrates that textural maturity does not change with lateral position in the inner parts of the intrusion.

### Principles of heat transfer in igneous cumulates

Enthalpy is a key variable for understanding melting and crystallization in the Earth. For example, in decompression melting an isentropic equilibrium is defined by a state of minimum enthalpy (Stolper & Asimow, 2007, in press). In the case of a crystallizing magma body, where entropy is maximized, the boundary conditions more closely approximate a controlled enthalpy ramp than a controlled thermal ramp. Enthalpy is a particularly important variable for consideration in the case of cumulates formed in a fractionating magma chamber. In such a body it is common to find a sequence of newly crystallizing phases as the bulk magma becomes sequentially saturated in, for example, olivine, plagioclase, augite, Fe–Ti oxide minerals, immiscible sulphide liquids, and apatite.

Wyllie (1963) noticed that as a fractionating liquid becomes saturated in each new phase, the liquidus slope becomes flatter. As a result, more crystals are produced

for a given decrement in temperature, and there is an increase in the ratio of latent heat to sensible heat extracted. The application of this principle to the discussion of cumulate maturation requires the definition of some terms.

We may define the fractional latent heat =  $H_f/H_{\text{Syst}}$ , where  $H$  is the enthalpy,  $H_f$  is the latent heat of fusion, and  $H_{\text{Syst}}$  is the enthalpy of the system. When the system cools, the total enthalpy is considered to be released to the surroundings in a regular continuum of heat loss described by the heat equation. At each addition of a new phase in the crystallizing assemblage, the newly flattened liquidus slope causes a discontinuous jump in the fractional latent heat, to a limit of 1.0 at a true eutectic or minimum where crystallization may proceed isothermally. The increase in the fractional latent heat has an effect on the possibilities for maturation of the cumulate, because it is a local heat source.

We may define the crystal productivity as the ratio  $x/T$ , where  $x$  is the amount of crystallization for a given incremental change in temperature  $T$ . As the slopes flatten in the Wyllie sequence, the relative efficiency of crystallization increases, and with it the crystal productivity, which in the limit (at a true eutectic) reaches infinity as  $\Delta T$  goes to zero. For convenience, we define the specific cooling rate as the inverse of the crystal productivity,  $T/x$ , which goes to zero at a true eutectic or a minimum. The specific cooling rate thus diminishes discontinuously at each change of slope in the Wyllie sequence.

A further dimension to fractional crystallization is the progress of reaction in the binary solution components of plagioclase and mafic minerals. These components fractionate CaAl toward pure NaSi and Mg toward pure Fe, respectively. As they do so, they tend to form quasi-isothermal tails to the total solid composition, and these tails potentially result in a significant volume of near-end-member residue at the latest, nearly isothermal, stages of crystallization (Maaløe, 1984; Morse, 1994, fig. 6.4a and 6.4b), described as thermal arrest in metallurgical systems (see Morse, 1997). As a result, the last stages of cumulate crystallization, whether intercumulus or megascopic in scale, may contain a significant fraction of evolved material crystallized at a fractional latent heat of nearly 1.0 and a specific cooling rate near zero. These principles also have potential application to the interpretation of the maturation (or lack thereof) in cumulates.

### Stepwise increases in textural maturity

The new observations demonstrate that the textural maturity of the Skaergaard gabbros increases stepwise at the base of LZc (Fig. 4) in a similar fashion to that already observed in LZa (Holness *et al.*, 2007a). Following Holness *et al.* (2007a), we suggest that this reflects a stepwise increase in the fractional latent heat as a result of a decrease in the slope of the liquidus associated with

the appearance of a new crystalline phase on the liquidus. This results in a greater opportunity for textural maturation and thus a stepwise increase in the median value of  $\Theta_{\text{cpp}}$

Holness *et al.* (2007a) suggested that the stepwise increase at ~540 m (Fig. 4) reflects the onset of clinopyroxene crystallization in the bulk magma. We suggest that the similar stepwise increase in textural maturity at the base of LZc corresponds to the arrival of Fe–Ti oxides as liquidus phases in the main body of the magma. Furthermore, the increase in  $\Theta_{\text{cpp}}$  at the base of UZb is caused by the onset of cumulus apatite crystallization. The short-lived nature of the high  $\Theta_{\text{cpp}}$  associated with apatite is discussed in a later section.

### The cumulus status of oxide grains

The considerable debate about the liquid line of descent for Skaergaard revolves around the issue of whether and/or when the residual liquid became enriched in Fe. Critical to this debate is the timing of the arrival of magnetite and ilmenite on the liquidus. A relatively early arrival of Fe–Ti oxide minerals, as initially suggested by Wager & Deer (1939), could mean that the liquid line of descent was characterized by iron and titanium depletion and silica enrichment (Hunter & Sparks, 1987, 1990), although others have suggested that progressive Fe enrichment is still possible even with an early advent of liquidus Fe–Ti oxides (Wager & Deer, 1939; Wager, 1960; McBirney & Naslund, 1990; Morse, 1990; McBirney, 1996; Tegner, 1997; Thy *et al.*, 2006).

The resolution of this problem has been hindered by uncertainty concerning the status of Fe–Ti oxides in the Layered Series. Wager & Brown (1968) suggested that ilmenite has cumulus status in LZa, although Irvine *et al.* (1998) suggested that the euhedral grains of ilmenite below LZc crystallized from the interstitial liquid in the mush. Jang *et al.* (2001) and Jang & Naslund (2003) suggested that magnetite below the upper parts of MZ is interstitial and crystallized from downwards-percolating evolved Fe-rich liquids. McBirney (1998) suggested that the abundant Fe–Ti oxide minerals present from the base of LZc crystallized from an isolated pool of Fe-rich magma on the floor of the chamber, rather than in the main magma reservoir.

The new data demonstrate a stepwise increase in textural maturity at the base of LZc (Fig. 4), and confirm the arrival of Fe–Ti oxides as a liquidus phase in the main body of the magma at this level in the intrusion, consistent with the conclusion of Irvine *et al.* (1998) and also with the field observation of concentration of Fe–Ti oxides in layers from this point in the stratigraphy. Importantly, there is only a single identifiable stepwise change in textural maturity which can be related to Fe–Ti oxides, suggesting the simultaneous, or near-simultaneous, arrival of ilmenite and magnetite on the liquidus. This is consistent with

an oxygen fugacity at, or close to, the fayalite–magnetite–quartz buffer (FMQ) at this point (Morse, 1980; Thy & Lofgren, 1994; Toplis & Carroll, 1995; Ariskin, 2002).

### Was Skaergaard replenished after LZa times?

Although Skaergaard is generally held to be the exemplar of closed-system fractionation, several attempts have been made to suggest that the intrusion was open at various times during its crystallization history (Hunter & Sparks, 1987; Stewart & DePaolo, 1990; McBirney, 2002). Stewart & DePaolo (1990) suggested, on the basis of variations in strontium isotope ratios, that the Skaergaard chamber may have been replenished by either a continuous series of pulses throughout the first 75% of crystallization, or a more localized series of pulses with one in MZ times and another in UZb times. McBirney (2002) made a tentative suggestion that magma was injected at MZ times, on the basis of the onset of sulphide precipitation (Bird *et al.*, 1991; Andersen *et al.*, 1998), the sudden increase in the rate of enrichment of the included elements, and what he mistakenly construed as an abrupt decrease of oxygen fugacity (Morse *et al.*, 1980). A 4 m wide, north–south-trending, compositionally primitive dyke that appears in LZa and disappears in MZ is suggested as a plausible conduit for such an injection, although later consideration of Sr and Nd isotopes led him to rule out a major influx of magma through the dyke (McBirney & Creaser, 2003).

Hunter & Sparks (1987) suggested that the absence of any significant quantity of highly evolved silicic liquid could be a consequence of tapping of liquids from the chamber, although Jang & Naslund (2001) pointed out that trace element concentrations in plagioclase preclude this. Volcanic eruptions fed by significant quantities of liquid from the chamber, and hence reduction in the size of the magma body, may result in a more rapid cooling and thus lower textural maturity. Although textural maturation certainly does effectively cease during the later stages of crystallization, the continuity of mineral compositional trends (e.g. McBirney, 1996) suggests that eruption was not the cause.

Previous work on the Cambridge drill core has demonstrated that pulsed filling of the magma chamber can be detected as positive excursions in textural maturity (Holness *et al.*, 2007a). Several such replenishment events are recorded in HZ, with the last occurring at the base of LZa (Fig. 4). Isolated positive excursions, apart from those that can be directly attributed to the onset of crystallization of new liquidus phases, are absent from the new dataset. However, the replenishment-related positive excursions in HZ typically involve ~20 m of stratigraphy. Although we do not have sufficient sample spacing over most of MZ to completely rule out the possibility of chamber replenishment, median  $\Theta_{\text{cpp}}$  is remarkably constant throughout MZ and the lower parts of UZa (Fig. 4).

It is unlikely that we could have completely avoided any thermal excursions with what effectively is a randomly chosen sample set. It appears that the Skaergaard magma chamber was indeed closed to further injection, and probably also to eruption, after LZa times, consistent with observations of smoothly changing mineral compositions (e.g. Tegner, 1997).

### The loss of thermal information in UZb

Median  $\Theta_{\text{cpp}}$  decreases to 73–80° in UZb (Fig. 4). This range is identical to that of the postulated floor chill zone at the base of the Cambridge drill core (Holness *et al.*, 2007a) and represents an almost complete cessation of pyroxene–plagioclase grain boundary migration above this level in the Layered Series (Fig. 3f). There are two possible reasons for the cessation of textural maturation at pyroxene–plagioclase three-grain junctions. The first is that the temperature of the remaining liquid dropped below the closure temperature for dihedral angle change, and the second is that the enthalpy loss from the system as a function of time increased significantly.

If the cessation of textural maturation was due to a general cooling of the intrusion, then we can place a maximum constraint on the closure temperature by considering the liquidus temperature of the remaining liquid. This will necessarily be higher than the temperature at the base of the mush (i.e. the solidification front), but the latter cannot be easily constrained without a detailed understanding of the progressive occlusion of porosity in the crystal mush. This is because the extent of exchange with the bulk liquid controls the extent of fractionation, and hence the liquidus temperature of the remaining melt, within the progressively solidifying mush.

A compilation of calculated and experimental liquidus temperatures from the published literature on the Layered Series is given in Table 2 and shown graphically in Fig. 5.

There is considerable agreement in the various experimental (McBirney & Naslund, 1990; Toplis & Carroll, 1995; Thy *et al.*, 2006) and calculated liquidus temperatures (Larsen *et al.*, 1989; Ariskin, 2002; Morse, 2007), with the exception of the calculations of Morse *et al.* (1980), which result in significantly higher temperatures for the lower Layered Series. The best-fit line through all data, apart from those of Morse *et al.* (1980), is shown in Fig. 5. Liquidus temperatures decrease steadily through LZ, but remain relatively constant in MZ [termed a ‘liquidus shelf’ by Wyllie (1963)]. The liquidus temperature decreases again from UZa, with a steep decline in UZb and UZc. This pattern is reflected in the variations in textural maturity in the Layered Series below UZb (Fig. 4).

Textural maturity reflects the time-integrated thermal history. In a closed solidifying system in which controls on total enthalpy loss to the surroundings remain constant (i.e. no late onset of hydrothermal convection and no changes of convective regime in the bulk magma), the textural maturity is controlled by the time for which any given horizon remains above the closure temperature for dihedral angle change. If this closure temperature is constant, then the liquidus temperature is a good proxy for the time-integrated thermal history. Although the variations in textural maturity through the Layered Series are complicated by superimposed step-changes associated with changes in the liquidus assemblage, comparison of Figs 4 and 5 shows that the decline in textural maturity through LZb is reflected in the relatively steep decline in liquidus temperature through LZa and LZb. The constancy of

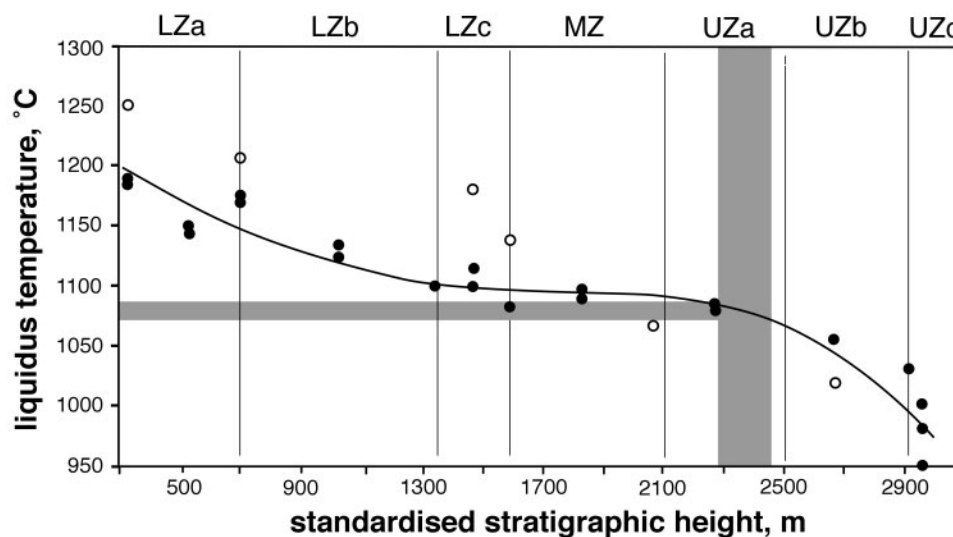


**Fig. 5.** Published experimental and calculated liquidus temperatures (given in Table 2) plotted as a function of standardized stratigraphic height.  $\circ$ , data of Morse *et al.* (1980), which are not included in the calculated line of best fit. The shaded boxes give the stratigraphic height at which textural maturation of pyroxene–plagioclase–plagioclase junctions ceases—this corresponds to a liquidus temperature of  $\sim 1075^{\circ}\text{C}$ .

textural maturation through MZ corresponds to a relatively constant liquidus temperature. The cessation of dihedral angle change in the Upper Zone corresponds to a significant and relatively steep decrease in liquidus temperature and occurs when the temperature at the top of the mush is  $\sim 1075^{\circ}\text{C}$ . As temperatures in the bulk liquid will be higher (by some unknown quantity) than that of the level at which no further clinopyroxene growth occurs (i.e. the base of the mush), this is an upper estimate for the closure temperature.

The cessation of textural maturation occurs in the same region of the stratigraphy as the loss of pronounced modal and grain-size layering, which, after becoming more distinct and well defined upwards in the stratigraphy, becomes insignificant near the middle of UZb (Boudreau and McBirney, 1997; Wager & Brown, 1968; McBirney, 1996; Irvine *et al.*, 1998). This loss of layering has been correlated with differences in rare earth element composition of plagioclase of the UZ compared with those of the Upper Border Series and used as evidence for cessation of chamber-wide convection (Jang & Naslund, 2001). It is intriguing that there is independent evidence supporting a significant change in the rate and mode of heat loss from the intrusion as it moves from a convective to a conductive regime at the same level as the loss of textural maturation. However, it is likely that the cessation of convection and onset of conductive heat loss would result in the reduction of heat loss rather than the increase suggested by the dihedral angles.

The effect of convection may, however, be recorded in the noise levels of the dihedral angle signature. Median  $\Theta_{\text{cpp}}$  is very smooth in lower UZa (in which it varies by  $<1^{\circ}$  from the average at any point), compared with LZb (where it varies by  $3^{\circ}$  around the average value). Large-scale, time-dependent, convection would result in temporally variable rates of heat loss if the size of the convective cells were of the order of the thickness of remaining liquid, and thus small-scale variations in the sub-solidus thermal history and  $\Theta_{\text{cpp}}$  might be expected. Conversely, steady-state conductive heat loss would result in a constant sub-solidus thermal history (albeit with a cooling trend) and less variation in median  $\Theta_{\text{cpp}}$ . Neither the scale of the effects of such processes nor the precise effect of such thermal fluctuation is known, however, rendering this hypothesis difficult to test.

Another possible player in the changing cooling rate of the Skaergaard intrusion is hydrothermal convection. The upper parts of Skaergaard are notable for the significantly reduced  $\delta^{18}\text{O}$  of plagioclase relative to inferred original igneous values (Taylor & Forester, 1979), as a result of large-scale convective circulation of meteoric ground waters in the permeable basalts that host the upper levels of the intrusion. The samples collected from Uttentals Plateau and Kramers  $\emptyset$  (Fig. 2) fall within the region of

normal  $\delta^{18}\text{O}$ , whereas those of UZ lie in progressively more strongly altered zones of the intrusion (Taylor & Forester, 1979, fig. 8). For an enhanced cooling rate caused by fluid circulation to have had a significant effect on the textural maturation process the water must have entered before the gabbros had moved through the temperature window for dihedral angle change. Thermal modelling of the circulation points to the bulk of the alteration occurring above  $500^{\circ}\text{C}$  (Norton & Taylor, 1979), and synchronously with exsolution of Ca-poor pyroxene from augite (Taylor & Forester, 1979). Minimum temperatures calculated for early hydrothermal veins are  $500\text{--}750^{\circ}\text{C}$  (Manning & Bird, 1986). However, because hydrothermal circulation requires a hydrostatic pressure and thus a fracture system, it cannot have occurred while there was any significant quantity of silicate liquid present (Taylor & Forester, 1979). Holness *et al.* (2005) demonstrated that the bulk of dihedral angle variation occurs synchronously with growth of pyroxene from silicate liquid, and thus we suggest that hydrothermal circulation in Skaergaard post-dated textural maturation. The reduction in textural maturation in UZ was therefore not a consequence of enhanced hydrothermal circulation in this part of the intrusion.

In summary, neither hydrothermal convection nor a change in the convective regime of the solidifying magma are plausible candidates for the cessation of textural maturity in the upper parts of the Layered Series. This is most probably a consequence of the temperature of the remaining liquid falling below the closure temperature for pyroxene–plagioclase grain boundary migration.

A final point can be made concerning the wide variation in median  $\Theta_{\text{cpp}}$  in samples lying above the horizon at which textural maturation effectively ceased. In samples for which the liquidus temperature was close to the closure temperature, or that were rapidly cooled (i.e. in a chill zone), any small variation in thermal history between samples will be manifest as a relatively large difference in median  $\Theta_{\text{cpp}}$ . This is because the earliest stages of textural maturation, when the median angle is far from solid-state equilibrium, are very sensitive to variations in temperature. As the median angle becomes larger, and closer to equilibrium, so the driving force becomes lower, and the sensitivity of the angle to changes in temperature (and thus sub-solidus thermal history) becomes lower, leading to a greater uniformity of final median  $\Theta_{\text{cpp}}$ . For the UZ rocks in which the angles are close to the inherited impingement values, small variations in thermal history are magnified into a large variation in textural maturity, leading to a wide range of median  $\Theta_{\text{cpp}}$  relative to that observed in rocks with much greater textural maturity.

### The thickness of the crystal mush

The thickness of the mush is an important variable, with consequences for mass transport and rheology, and is

Table 3: Published estimates of liquidus temperatures ( $^{\circ}\text{C}$ ) for the Layered Series of the Skaergaard intrusion

	Larsen <i>et al.</i> (1989)	Ariskin (2002)	Thy <i>et al.</i> (2006)	McBirney & Naslund (1990)	Toplis & Carroll (1995)	Morse <i>et al.</i> (1980)	Morse (2007)	Lindsley <i>et al.</i> (1969)
LZa	1180 (b)	1145 (c)		1150 (c)		1250 (b)	1191 (b)	
LZb		1124 (c)	1154 (b)	1135 (c)	1130 (b)	1208 (b)	1173 (b)	
LZc		1100 (c)	1102 $\pm$ 5 (b)	1115 (c)	1100 (b)	1180 (b)		
MZ		1090 (c)	1084 $\pm$ 6 (b)	1097 (c)		1139 (b)		
UZa		1085 (c)		1082 (c)		1090 (b)		
UZb				1056 (c)				
UZc				1002 (c)			1040 (b)	980–950

Indication is given whether the estimate applies to the base (b) of the division or the centre (c). The estimates of Morse *et al.* (1980), Larsen *et al.* (1989), Ariskin (2002) and Morse (2007) are calculated, whereas those of McBirney & Naslund (1990), Toplis & Carroll (1995) and Thy *et al.* (2006) are experimentally determined. The estimate of Lindsley *et al.* (1969) was based on considerations of observed phase equilibria.

itself controlled by the relative permeability of the mush to both heat and liquid. One end-member is that of the hard-ground, in which adcumulates form at an abrupt interface between essentially fully solidified rock and the bulk liquid (e.g. Morse, 1986). The other end-member involves a very thick mush in which the proportion of solid phases decreases from 100% to 0% over a distance of perhaps several hundreds of metres (e.g. Tait & Jaupart, 1992). The data presented here offer an opportunity to constrain the thickness of the Skaergaard mush, at least in the vicinity of the step-change at 540 m stratigraphic height (within LZa) where the samples are closely spaced.

The step-change at 540 m is associated with the arrival of clinopyroxene on the liquidus in the bulk liquid, and occurs over  $\sim 1$  m of stratigraphy. Cumulates at the level represented by the bottom of the step did not experience the change in specific latent heat associated with the onset of liquidus clinopyroxene crystallization and thus had just cooled to the closure temperature. Cumulates at the level represented by the top of the step are those that experienced the full effects of liquidus clinopyroxene crystallization and were thus at the top of the mush at that time. Experimental determinations of the temperature of the bulk liquid when clinopyroxene joins the assemblage range from 1154 $^{\circ}\text{C}$  to 1208 $^{\circ}\text{C}$  (Table 3), although we consider temperatures in the middle of this range to be the most likely (i.e. 1180 $^{\circ}\text{C} \pm 15^{\circ}\text{C}$ ). In the previous section we suggested that 1075 $^{\circ}\text{C}$  is a plausible maximum estimate of the closure temperature for dihedral angle change at clinopyroxene–plagioclase–plagioclase junctions, which results in a thermal gradient within the upper parts of the mush of 90–120 $^{\circ}\text{C}/\text{m}$ . If the closure temperature were 200 $^{\circ}\text{C}$  lower (for example), this gradient would increase to 290–320 $^{\circ}\text{C}/\text{m}$ .

The thickest possible mush would be one in which the interstitial liquid was isolated and could evolve all the way to the granitic minimum which, for LZa–b, is likely to be at 680 $^{\circ}\text{C}$  (Larsen & Tegner, 2006). Assuming the thermal gradient were linear through the mush this leads to a distance of 4.3–5.4 m (assuming a closure temperature of 1075 $^{\circ}\text{C}$ ) from the bulk liquid to the level at which the rock is 100% solidified. This distance decreases to 1.5–1.7 m for a closure temperature of 875 $^{\circ}\text{C}$ . A mush with a more adcumulate nature, in which the last liquid present was less evolved than the granitic minimum, would be thinner.

Although these estimates are necessarily crude simplifications, it is clear that solidification of the Skaergaard intrusion most closely approximated the hard-ground model of Morse (1986). This is consistent with the scale of slumping and the mechanically disrupted zones surrounding fallen blocks (Irvine *et al.*, 1998).

### Oversaturation prior to arrival of new liquidus phases

The new data presented here are notable for the decrease in textural maturity through LZc towards a plateau in MZ, and the abrupt decrease in textural maturity closely following the onset of apatite crystallization defining the base of UZb (Fig. 4). We suggest that both may be the result of significant oversaturation of the bulk liquid before nucleation of both Fe–Ti oxides and apatite. Once nucleated, a consequent burst of crystallization of the new phase temporarily increased the fractional latent heat.

The onset of apatite nucleation occurred once textural maturation had begun to decline, and resulted in a remarkable thermal disturbance recorded as a spike in median  $\Theta_{\text{cpp}}$ . We suggest that this was induced by a temporary abundance of apatite crystallization as a result of

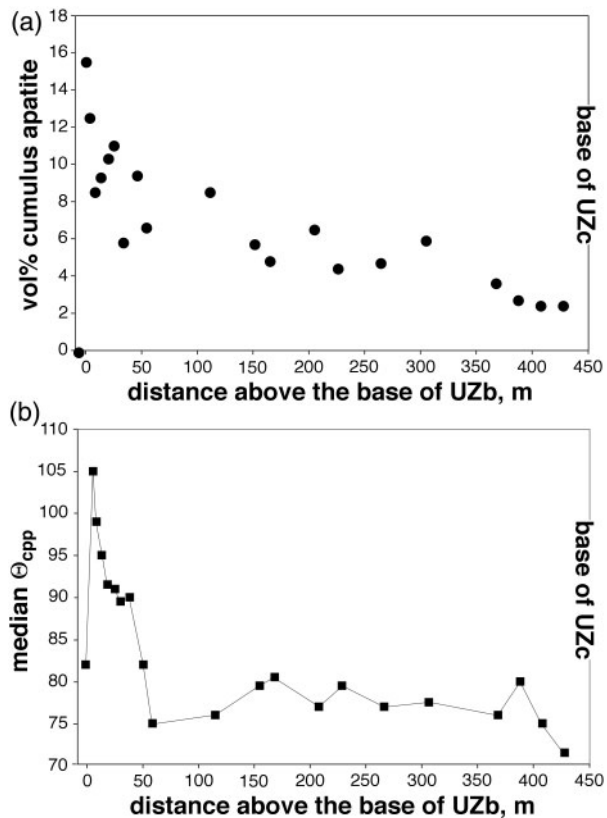


**Fig. 6.** (a) Volumetric proportion of cumulus apatite in UZb as a function of actual stratigraphic height measured in the 90-22 drill core. (b) Median  $\Theta_{cpp}$  in UZb as a function of actual stratigraphic height measured in the 90-22 drill core.

significant overstepping of apatite nucleation. Once apatite had begun to crystallize, this temporary abundance of apatite growth increased the fractional latent heat sufficiently to permit median  $\Theta_{cpp}$  to achieve values of  $105^\circ$ . After reduction of the temporary supersaturation the steady-state rate of crystallization on the evolved apatite-bearing multi-phase cotectic was insufficient to permit any significant movement of clinopyroxene–plagioclase grain boundaries, and textural maturation effectively ceased.

The volume per cent of cumulus apatite decreases with stratigraphic height within UZb (Wager, 1963; Fig. 6a). This is because apatite becomes a liquidus phase at about 1%  $P_2O_5$  in a basic liquid (Green & Watson, 1982) and the resultant cumulates contain more P than the liquid. The liquid therefore crystallizes less and less apatite (Wager, 1960; Tegner *et al.*, 2006). However, the lowermost samples from UZb in core 90-22 contain almost 16 vol. % apatite, and we suggest that this records the stratigraphically localized overabundance of apatite crystallization resulting from the overstep. The latent heat release associated with this abundant apatite crystallization reduced the specific cooling rate sufficiently to permit median

$\Theta_{cpp}$  to reach  $105^\circ$  (Fig. 6b). Once the apatite in the cumulates was reduced to about 8–10 vol. %, the latent heat release was temporarily sufficient to maintain textural maturity with  $\Theta_{cpp}$  of  $\sim 90^\circ$  for a few tens of metres of additional cumulate, although the continuing reduction in temperature of the cooling intrusion (Fig. 5) meant that eventually (within 50 m of the onset of apatite crystallization) even this latent heat contribution became inadequate for significant plagioclase–pyroxene grain boundary migration. Textural maturation is effectively non-existent in the overlying horizons.

It is notable that there is no localized over-shoot of the elevated  $\Theta_{cpp}$  associated with the arrival of cumulus clinopyroxene (Fig. 4), and that the over-shoot for Fe–Ti oxides is less pronounced than that for apatite: the extent of the supersaturation, and hence over-shoot, increases as the liquid becomes more evolved. Wyllie (1963) pointed out that when the liquidus path is steep, the liquid temperature must fall far below the liquidus to produce much supersaturation, whereas for gentle slopes a high degree of supersaturation can be produced when the liquid temperature falls only slightly below the liquidus. This means that as the liquidus slope is progressively reduced during fractionation it will become commensurately easier to create a transient peak in  $\Theta_{cpp}$  at the arrival of each new phase. Thus large supersaturations become more likely for successively arriving phases during closed-system fractionation. We suggest that this is recorded in the successively greater over-shoots of textural maturity in the Skaergaard Layered Series.

## CONCLUSIONS

Consideration of the extent to which inherited impingement textures have approached sub-solidus textural equilibrium in the vicinity of clinopyroxene–plagioclase–plagioclase junctions in intrusions for which cooling was sufficiently rapid to prevent full attainment of textural equilibrium demonstrates the accessibility of subtle variations in their cooling record. The arrival of new phases on the liquidus exerts a control on the relative contribution of latent heat to the enthalpy loss of the system, reducing the specific cooling rate and thus causing a measurable increase in textural maturity of the resultant cumulates. The generality of this process of stepwise changes in specific cooling rate may have important implications for the details of porosity occlusion in the mush. Although our data suggest that the cumulates were completely solid only a few metres below the top of the mush, the gradual change from an orthocumulate towards a more adcumulate character with height in the Skaergaard intrusion (Wager *et al.*, 1960), reflecting an increase in post-accumulation growth of primocrysts, may have resulted from the progressive changes in the rate of accumulation of crystals recorded by  $\Theta_{cpp}$ .

The Skaergaard magma began crystallizing ilmenite and magnetite simultaneously at the base of LZc, consistent with an oxygen fugacity at the FMQ buffer at this level in the intrusion. The arrival of both Fe–Ti oxides and apatite as liquidus phases was accompanied by oversaturation of the magma in the bulk of the chamber, detectable by transient positive excursions in textural maturity resulting from a burst of crystallization.

Textural maturation ceased in the upper parts of the Skaergaard Layered Series, most probably as a consequence of the entire intrusion cooling through the closure temperature for two-phase grain boundary migration. This means that there is no record of variations in sub-solidus thermal history above this point in the stratigraphy. A corollary of this is that the use of pyroxene–plagioclase–plagioclase dihedral angles as a record of thermal history may be limited to mafic intrusions of at least the size of Skaergaard, or to smaller ones intruded at greater depth in the crust.

## ACKNOWLEDGEMENTS

We acknowledge the contributions of Charles Leshner, Peter Thy, Jakob Jakobsen, Joel Simpson and Anja Fonseca to fieldwork in 2000, which was funded by the Danish Natural Sciences Research Council. M.B.H. and G.S. are grateful to Minik Rosing for hospitality during a visit to Copenhagen. G.S. acknowledges a NERC CASE studentship in collaboration with Galahad Gold plc. We are indebted to Michael Carpenter for discussions of the pyroxene textures, and to A. McBirney and A. Boudreau for helpful reviews that improved the manuscript.

## SUPPLEMENTARY DATA

Supplementary data for this paper are available at *Journal of Petrology* online.

## REFERENCES

- Andersen, J. C. Ø., Rasmussen, H., Nielsen, T. F. D. & Ronsbø, J. G. (1998). The Triple Group and the Platinova gold and palladium reefs in the Skaergaard intrusion: Stratigraphic and petrographic relations. *Economic Geology and the Bulletin of the Society of Economic Geologists* **93**, 488–509.
- Ariskin, A. A. (2002). Geochemical thermometry of the Layered Series rocks of the Skaergaard intrusion. *Petrology* **10**, 495–518.
- Batiza, R. & Vanko, D. A. (1985). Petrologic evolution of large failed rifts in the Eastern Pacific—petrology of volcanic and plutonic rocks from the Mathematician Ridge area and the Guadalupe Trough. *Journal of Petrology* **26**, 564–602.
- Bird, D. K., Brooks, C. K., Gannicott, R. A. & Turner, P. A. (1991). A gold-bearing horizon in the Skaergaard intrusion, East Greenland. *Economic Geology* **86**, 1083–1092.
- Bollingberg, K. (1995). Textural and chemical evolution of the Fe–Ti oxide minerals during the late- and post-magmatic cooling of the Skaergaard intrusion, East Greenland. PhD thesis, University of Copenhagen.
- Boorman, S., Boudreau, A. & Kruger, F. J. (2004). The Lower Zone–Critical Zone transition of the Bushveld Complex: a quantitative textural study. *Journal of Petrology* **45**, 1209–1235.
- Boudreau, A. E. & McBirney, A. R. (1997). The Skaergaard Layered Series. Part III. Non-dynamic layering. *Journal of Petrology* **38**, 1003–1020.
- Bown, M. G. & Gay, P. (1960). An X-ray study of exsolution phenomena in the Skaergaard pyroxenes. *Mineralogical Magazine* **32**, 379–388.
- Brey, G. P. & Kolher, T. (1990). Geothermobarometry in four-phase lherzolites II. New thermobarometers and practical assessment of existing thermobarometers. *Journal of Petrology* **31**, 1353–1378.
- Brooks, C. K. & Nielsen, T. F. D. (1982). The Phanerozoic development of the Kangerdlugssuaq area, East Greenland. *Meddelelser om Grønland, Geoscience* **9**, 1–30.
- Brooks, C. K. & Nielsen, T. F. D. (1990). A discussion of Hunter & Sparks. *Contributions to Mineralogy and Petrology* **104**, 244–247.
- Brothers, R. N. (1964). Petrofabric analysis of Rhum and Skaergaard layered rocks. *Journal of Petrology* **5**, 255–274.
- Brown, G. M. (1957). Pyroxenes from the early and middle stages of fractionation of the Skaergaard Intrusion, East Greenland. *Mineralogical Magazine* **31**, 511–543.
- Brown, G. M. (1972). Pigeonitic pyroxenes: a review. In: Shagam, R., Hargraves, R. B., Moran, W. J., Van Houten, F. B., Burk, C. A., Holland, H. D. & Hollister, L. C. (eds) *Studies in Earth and Space Sciences: A Memoir in Honor of Harry Hammond Hess*. *Geological Society of America* **132**, 523–534.
- Bulau, J. R., Waff, H. S. & Tyburczy, J. A. (1979). Mechanical and thermodynamic constraints on fluid distribution in partial melts. *Journal of Geophysical Research* **84**, 6102–6108.
- Campbell, I. H. (1978). Some problems with the cumulus theory. *Lithos* **11**, 311–323.
- Champness, P. E. & Copley, P. A. (1976). The transformation of pigeonite to orthopyroxene (in electron microscopy in mineralogy). In: Wenk, H. R. & Thomas, G. (eds) *Applications of Electron Microscopy in Mineralogy*. Berlin: Springer-Verlag, pp. 229–233.
- Copley, P. A. (1973). Electron microprobe studies of phase transformations in pyroxene minerals. PhD thesis, University of Manchester.
- Copley, P. A. & Champness, P. E. (1975). The transformation of pigeonite to orthopyroxene. In: Venables, J. A. (ed.) *Developments in Electron Microscopy and Analysis*. London: Academic Press, pp. 475–476.
- Copley, P. A., Champness, P. E. & Lorimer, G. W. (1974). Electron petrography of exsolution textures in an iron-rich clinopyroxene. *Journal of Petrology* **15**, 41–57.
- Deer, W. A. (1976). Tertiary igneous rocks between Scoresby Sund and Kap Gustov Holm, East Greenland. In: Escher, A. & Watts, W. S. (eds) *Geology of East Greenland. Grønlands Geologiske Undersøgelse*, pp. 405–429.
- Elliott, M. T., Cheadle, M. J. & Jerram, D. A. (1997). On the identification of textural equilibrium in rocks using dihedral angle measurements. *Geology* **25**, 355–358.
- Green, T. H. & Watson, E. B. (1982). Crystallisation of apatite in natural magmas under high pressure hydrous conditions, with particular reference to 'orogenic' rock series. *Contributions to Mineralogy and Petrology* **79**, 96–105.
- Hanghøj, K., Rosing, M. T. & Brooks, C. K. (1995). Evolution of the Skaergaard magma: evidence from crystallised melt inclusions. *Contributions to Mineralogy and Petrology* **120**, 265–269.
- Harte, B., Pattison, D. R. M. & Linklater, C. M. (1991). Field relations and petrography of partially melted pelitic and semi-pelitic rocks.

- In: Völl, G., Töpel, J., Pattison, D. R. M. & Seifert, F. (eds) *Equilibrium and Kinetics in Contact Metamorphism: The Ballachulish Igneous Complex and its Aureole*. Heidelberg: Springer, pp. 181–210.
- Herring, C. (1951). Surface tension as a motivation for sintering. In: Kingston, W. E. (ed.) *Physics of Powder Metallurgy*. New York: McGraw-Hill, pp. 143–179.
- Higgins, M. D. (1998). Origin of anorthosite by textural coarsening: quantitative measurements of a natural sequence of textural development. *Journal of Petrology* **39**, 1307–1323.
- Holness, M. B. (2005). Spatial constraints on magma chamber replenishment events from textural observations of cumulates: the Rum Layered Intrusion, Scotland. *Journal of Petrology* **46**, 1585–1601.
- Holness, M. B. (2006). Melt–solid dihedral angles of common minerals in natural rocks. *Journal of Petrology* **47**, 791–800.
- Holness, M. B. (2007). Textural immaturity of cumulates as an indicator of magma chamber processes: infiltration and crystal accumulation in the Rum Layered Suite. *Journal of the Geological Society, London* **164**, 529–539.
- Holness, M. B. & Clemens, J. D. (1999). Partial melting of the Appin Quartzite driven by fracture-controlled H<sub>2</sub>O infiltration in the aureole of the Ballachulish Igneous Complex, Scottish Highlands. *Contributions to Mineralogy and Petrology* **136**, 154–168.
- Holness, M. B., Cheadle, M. J. & McKenzie, D. (2005). On the use of changes in dihedral angle to decode late-stage textural evolution in cumulates. *Journal of Petrology* **46**, 1565–1583.
- Holness, M. B., Nielsen, T. F. D. & Tegner, C. (2007a). Textural maturity of cumulates: a record of chamber filling, liquidus assemblage, cooling rate and large-scale convection in mafic layered intrusions. *Journal of Petrology* **48**, 141–157.
- Holness, M. B., Anderson, A. T., Martin, V. M., MacLennan, J., Passmore, E. & Schwindinger, K. (2007b). Textures in partially solidified crystalline nodules: a window into the pore structure of slowly cooled mafic intrusions. *Journal of Petrology* **48**, 791–800.
- Hunter, R. H. (1987). Textural equilibrium in layered igneous rocks. In: Parsons, I. (ed.) *Origins of Igneous Layering*. Dordrecht: D. Reidel, pp. 473–503.
- Hunter, R. H. & Sparks, R. S. J. (1987). The differentiation of the Skaergaard intrusion. *Contributions to Mineralogy and Petrology* **95**, 451–461.
- Hunter, R. H. & Sparks, R. S. J. (1990). The differentiation of the Skaergaard intrusion. Reply to A. R. McBirney and H. R. Naslund. *Contributions to Mineralogy and Petrology* **104**, 248–254.
- Irvine, T. N. (1982). Terminology for layered intrusions. *Journal of Petrology* **23**, 127–162.
- Irvine, T. N., Andersen, J. C. Ø. & Brooks, C. K. (1998). Included blocks (and blocks within blocks) in the Skaergaard intrusion: geological relations and the origins of rhythmic modally graded layers. *Geological Society of America Bulletin* **110**, 1398–1447.
- Jang, Y. D. & Naslund, H. R. (2001). Major and trace element composition of the Skaergaard plagioclase; geochemical evidence for changes in magma dynamics during the final stage of crystallisation of the Skaergaard intrusion. *Contributions to Mineralogy and Petrology* **140**, 441–457.
- Jang, Y. D. & Naslund, H. R. (2003). Major and trace element variation in ilmenite in the Skaergaard intrusion: petrologic implications. *Chemical Geology* **193**, 109–125.
- Jang, Y. D., Naslund, H. R. & McBirney, A. R. (2001). The differentiation trend of the Skaergaard intrusion and the timing of magnetite crystallisation: iron enrichment revisited. *Earth and Planetary Science Letters* **189**, 189–196.
- Kretz, R. (1966). Interpretation of the shape of mineral grains in metamorphic rocks. *Journal of Petrology* **7**, 68–94.
- Laporte, D. & Provost, A. (2000). Equilibrium geometry of a fluid phase in a polycrystalline aggregate with anisotropic surface energies: Dry grain boundaries. *Journal of Geophysical Research* **105**, 25937–25953.
- Larsen, L. M., Watt, W. S. & Watt, M. (1989). Geology and petrology of the Lower Tertiary plateau basalts of the Scoresby Sund region, East Greenland. *Bulletin Grønlands Geologiske Undersøgelse* **157**, 164.
- Larsen, R. B. & Tegner, C. (2006). Pressure conditions for the solidification of the Skaergaard intrusion: eruption of East Greenland flood basalts in less than 300,000 years. *Lithos* **92**, 181–197.
- Lindsley, D. H., Brown, G. M. & Muir, I. D. (1969). Conditions of the ferrowollastonite–ferrohedenbergite inversion in the Skaergaard Intrusion, East Greenland. In: *Mineralogical Society of America, Special Papers*, **2**, 193–201.
- Maaløe, S. (1976). Zoned plagioclase of the Skaergaard Intrusion, East Greenland. *Journal of Petrology* **17**, 398–419.
- Maaløe, S. (1984). Fractional crystallization and melting within binary systems with solid solution. *American Journal of Science* **284**, 272–287.
- Manning, C. E. & Bird, D. K. (1986). Hydrothermal clinopyroxenes of the Skaergaard intrusion. *Contributions to Mineralogy and Petrology* **92**, 437–447.
- Marsh, B. D. (2006). Dynamics of magmatic systems. *Elements* **2**, 287–292.
- McBirney, A. R. (1989). *Geological map of the Skaergaard Intrusion, East Greenland, scale 1:20 000*. Eugene: Department of Geology: University of Oregon.
- McBirney, A. R. (1996). The Skaergaard intrusion. In: Cawthorn, R. G. (ed.) *Layered Intrusions*. Amsterdam: Elsevier Science B.V., pp. 147–180.
- McBirney, A. R. (1998). Is the cumulate paradigm at risk?: a reply. *Journal of Geology* **106**, 370–371.
- McBirney, A. R. (2002). The Skaergaard Layered Series. Part VI. Excluded trace elements. *Journal of Petrology* **43**, 535–556.
- McBirney, A. R. & Creaser, R. A. (2003). The Skaergaard Layered Series, Part VII: Sr and Nd isotopes. *Journal of Petrology* **44**, 757–771.
- McBirney, A. R. & Hunter, R. H. (1995). The cumulate paradigm reconsidered. *Journal of Geology* **103**, 114–122.
- McBirney, A. R. & Naslund, H. R. (1990). The differentiation of the Skaergaard intrusion. A discussion of Hunter and Sparks (Contrib Mineral Petrol 95: 451–461). *Contributions to Mineralogy and Petrology* **104**, 235–247.
- McBirney, A. R. & Noyes, R. M. (1979). Crystallisation and layering of the Skaergaard Intrusion. *Journal of Petrology* **20**, 487–554.
- Morse, S. A. (1980). Kiglapait mineralogy II: Fe–Ti oxide minerals and the activities of oxygen and silica. *Journal of Petrology* **21**, 685–719.
- Morse, S. A. (1986). Convection in aid of adcumulus growth. *Journal of Petrology* **27**, 1183–1214.
- Morse, S. A. (1990). A discussion of Hunter and sparks (Contrib Mineral Petrol 95: 451–461). *Contributions to Mineralogy and Petrology* **104**, 240–251.
- Morse, S. A. (1994). *Basalts and Phase Diagrams* (corrected and reprinted edition). Melbourne, FL: Krieger, 493 pp.
- Morse, S. A. (1997). Binary solutions and the lever rule revisited. *Journal of Geology* **105**, 471–482.
- Morse, S. A. (1998). Is the cumulate paradigm at risk?: an extended discussion of The cumulate paradigm reconsidered. *Journal of Geology* **106**, 367–370.
- Morse, S. A. (2007). Toward a thermal model for the Skaergaard liquidus. *Geological Society of America, Abstracts with Programs* **39**, 3–13.

- Morse, S. A., Lindsley, D. H. & Williams, R. J. (1980). Concerning intensive parameters in the Skaergaard Intrusion. *American Journal of Science* **280-A**, 159–170.
- Nielsen, T. F. D. (2004). The shape and volume of the Skaergaard Intrusion, East Greenland: implications for mass balance and bulk composition. *Journal of Petrology* **45**, 507–530.
- Nielsen, T. F. D., Tegner, C., Thy, P., Fonseca, A., Jakobsen, J. K., Kristensen, M., Simpson, J., Brooks, C. K., Kent, A. J. R., Peate, D. W. & Leshner, C. E. (2000). Retrieval of Platinova drill cores: A new Skaergaard initiative. *Transactions of the American Geophysical Union* **81**, Fall Meeting Supplement, V21E-15.
- Norton, D. & Taylor, H. P. (1979). Quantitative simulation of the hydrothermal systems of crystallising magmas on the basis of transport theory and oxygen isotope data: an analysis of the Skaergaard intrusion. *Journal of Petrology* **20**, 421–486.
- Nwe, Y. Y. (1976). Electron-probe studies of the earlier pyroxenes and olivines from the Skaergaard Intrusion, East Greenland. *Contributions to Mineralogy and Petrology* **55**, 105–126.
- Nwe, Y. Y. & Copley, P. A. (1975). Chemistry, subsolidus relations and electron petrography of pyroxenes from the late ferrodiorites of the Skaergaard intrusion, East Greenland. *Contributions to Mineralogy and Petrology* **53**, 37–54.
- Platten, I. M. (1981). Partial melting of feldspathic quartzite around late Caledonian minor intrusions in Appin, Scotland. *Geological Magazine* **119**, 413–419.
- Rosenberg, C. L. & Riller, U. (2000). Partial melt topology in statically and dynamically recrystallised granite. *Geology* **28**, 7–10.
- Sawyer, E. W. (1999). Criteria for the recognition of partial melting. *Physics and Chemistry of the Earth* **24**, 269–279.
- Sawyer, E. W. (2001). Melt segregation in the continental crust: distribution and movement of melt in anatectic rocks. *Journal of Metamorphic Geology* **19**, 291–309.
- Stewart, B. W. & DePaolo, D. J. (1990). Isotopic studies of processes in mafic magma chambers: II. The Skaergaard intrusion, East Greenland. *Contributions to Mineralogy and Petrology* **104**, 125–141.
- Stolper, E. M. & Asimow, P. (2007). Insights into mantle melting from graphical analysis of one-component systems. *American Journal of Science* (in press).
- Stripp, G., Holness, M. & Veksler, I. (2006). Enigmatic late-stage textures in mafic cumulates: Skaergaard Intrusion, East Greenland. *Transactions of the American Geophysical Union* **87**, Fall Meeting Supplement, V51B-1672.
- Tait, S. & Jaupart, C. (1992). Compositional convection in a reactive crystalline mush and melt differentiation. *Journal of Geophysical Research* **97**, 6735–6756.
- Taylor, H. P. & Forester, R. W. (1979). An oxygen and hydrogen isotope study of the Skaergaard intrusion and its country rocks: a description of a 55 m.y. old fossil hydrothermal system. *Journal of Petrology* **20**, 355–419.
- Tegner, C. (1997). Iron in plagioclase as a monitor of the differentiation of the Skaergaard intrusion. *Contributions to Mineralogy and Petrology* **128**, 45–51.
- Tegner, C., Duncan, R. A., Bernstein, S., Brooks, C. K., Bird, D. K. & Storey, M. (1998). Ar<sup>40</sup>–Ar<sup>39</sup> geochronology of Tertiary mafic intrusions along the East Greenland rifted margin: relation to flood basalts and the Iceland hotspot track. *Earth and Planetary Science Letters* **156**, 75–88.
- Tegner, C., Cawthorn, R. G. & Kruger, F. J. (2006). Cyclicity in the Main and Upper Zones of the Bushveld complex, South Africa: crystallisation from a zoned magma sheet. *Journal of Petrology* **47**, 2257–2279.
- Thomson, W. (1887). On the division of space with minimum partitional area. *Philosophical Magazine* **24**, 503–514.
- Thy, P. & Lofgren, G. E. (1994). Experimental constraints on the low-pressure evolution of transitional and mildly alkalic basalts: the effect of Fe–Ti oxide minerals and the origin of basaltic andesites. *Contributions to Mineralogy and Petrology* **116**, 340–351.
- Thy, P., Leshner, C. E., Nielsen, T. F. D. & Brooks, C. K. (2006). Experimental constraints on the Skaergaard liquid line of descent. *Lithos* **92**, 154–180.
- Toplis, M. J. & Carroll, M. R. (1995). An experimental study of the influence of oxygen fugacity on Fe–Ti oxide stability, phase relations, and mineral–melt equilibria in ferro-basaltic systems. *Journal of Petrology* **36**, 1137–1170.
- Vernon, R. H. (1968). Microstructures of high-grade metamorphic rocks at Broken Hill, Australia. *Journal of Petrology* **9**, 1–22.
- Vernon, R. H. (1970). Comparative grain-boundary studies of some basic and ultrabasic granulites, nodules and cumulates. *Scottish Journal of Geology* **6**, 337–351.
- Vernon, R. H. (1997). Comment: On the identification of textural disequilibrium in rocks using dihedral angle measurements. By Elliott, M. T. & Cheadle, M. J. *Geology* **25**, 1055.
- Wager, L. R. (1960). The major element variation of the layered series of the Skaergaard intrusion and a re-estimation of the average composition of the hidden series and of successive residual magmas. *Journal of Petrology* **1**, 364–398.
- Wager, L. R. (1963). The mechanism of adcumulus growth in the layered series of the Skaergaard intrusion. In: Fisher, D. J., Freuh, A. J., Hurlbert, C. S. & Tilley, C. E. (eds) *Symposium on Layered Intrusions. Mineralogical Society of America, Special Papers* **1**, 1–9.
- Wager, L. R. & Brown, G. M. (1968). *Layered Igneous Rocks*. San Francisco, CA: Freeman.
- Wager, L. R. & Deer, W. A. (1939). Geological investigations in East Greenland. Part III. The petrology of the Skaergaard intrusion, Kangerdlussuaq, East Greenland. *Meddelelser om Grønland* **105**.
- Wager, L. R., Brown, G. M. & Wadsworth, W. J. (1960). Types of igneous cumulates. *Journal of Petrology* **1**, 73–85.
- Wyllie, P. J. (1963). Effects of the changes in slope occurring on liquidus and solidus paths in the system diopside–anorthite–albite. *Mineralogical Society of America, Special Papers* **1**, 204–212.